J. Fluid Mech. (1982), *vol.* 121, *pp.* 517–529
Printed in Great Britain

Cambered valve leaflets that maximize initial rate of closure

By E. O. TUCK,
University of Adelaide, South Australia 5001
A. HELFGOTT
Flinders Medical Centre, South Australia 5042
AND R. W. YEUNG
Massachusetts Institute of Technology, Cambridge, MA 02139, U.S.A.

(Received 27 July 1981 and in revised form 15 December 1981)

Camber distributions are chosen for airfoils of zero thickness that maximize the angular velocity induced by a sudden decrease in free-stream velocity. Those optimal shapes that are in equilibrium in steady forward flow are also neutrally stable in that position.

1. Introduction

The task considered in this paper is that of the choice of the optimal camber for a pivoted thin airfoil near a plane boundary, in unsteady two-dimensional flow of an incompressible inviscid fluid, as sketched in figure 1. The aim of the optimization is to maximize the destabilizing moment about the pivot point, owing to deceleration of the incident flow. The work has possible application to the design of valves, especially those used for replacement of the valves of the heart.

A similar, but entirely steady, analysis was recently outlined by Tuck (1982; henceforth designated I). That is, the design in I was chosen so as to maximize the steady reversed-flow destabilizing moment, given that the leaflet is still in the open position, where it was in equilibrium in a previous steady forward flow. This procedure ignores the unsteady effects that take place as the flow changes its direction, and is somewhat unrealistic in that, if the valve is really doing the job it was designed to do, no steady reversed flow will ever occur.

Inclusion of unsteady-flow (in particular, vortex-shedding) effects on the dynamics of a pivoting airfoil of *given* camber, in a stream of time-varying speed, is not out of the question, and numerical computations of this nature have been performed (e.g. by Yeung 1978) in other contexts. However, the complexity of these computations is such that the prospect of using such numerical results to design the camber that maximizes some objective function is not very great.

In fact, we are not necessarily interested in a complete unsteady solution, and in particular (for very good reasons) we are not interested in solutions involving significant unsteady vortex shedding from the trailing edge. Again, if a significant amount of such vortex shedding occurs, the design must be a failure, at least for applications such as to prosthetic heart valves, where we must avoid vortices as far as possible, in order to prevent damage and clot formation in the blood.

Vortex shedding from an airfoil occurs in unsteady flow when the airfoil conforms

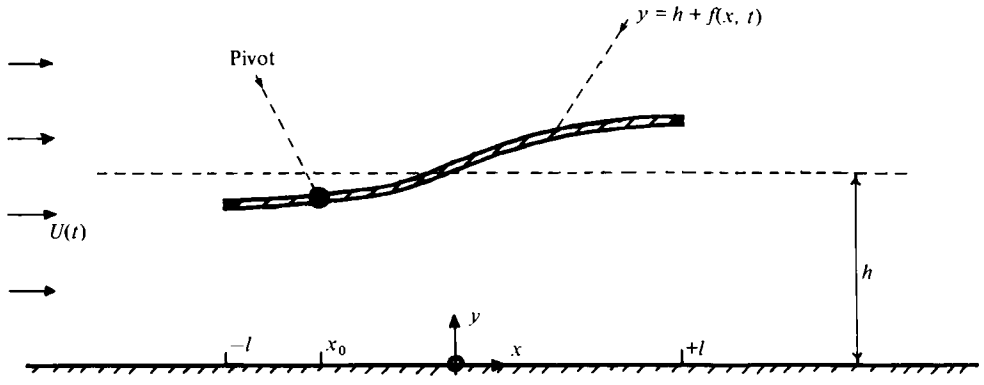

FIGURE 1. Sketch of flow situation.

insufficiently to the streamlines of the undisturbed flow. This is, of course, to be expected for a *fixed* airfoil with significant camber and/or angle of attack. If, on the other hand, the foil is allowed to move freely in response to fluid pressure, this extra freedom will enable it at least to attempt to conform to the undisturbed flow as it moves. Thus an optimally designed valve leaflet will minimize the extent of vortex shedding.

For example, a natural flexible heart valve can achieve this ideal performance almost exactly, since there is no reason in principle why it should not follow the paths of fluid particles quite closely. However, the single degree of freedom available to a rigid pivoting prosthetic valve leaflet allows only an 'averaged' flow alignment, and some vortex shedding is inevitable.

In the present paper we consider those unsteady flows in which vortex shedding can be neglected entirely. This can either be interpreted as an approximation to the ideal state discussed above, or as an exact treatment of the instantaneous response to a step-function change in the forward flow. If there is such a rapid alteration in the input flow conditions, the immediate response of the flow streamlines, and hence of the valve itself, is unaffected by vortex shedding, which occurs only over a longer time span.

In fact, the only unsteady flows in which we are interested are those that occur *quickly*. That is, we consider flows in which the valve perturbs a uniform stream $U(t)$, which suddenly decreases near $t = 0$ from a previous steady value $U = U_0$ to zero or nearly zero. As a result of this decrease there will be a moment acting about the pivot point, which will, if the valve is correctly designed, act to cause it to close.

Specifically, if $U(t)$ is exactly a step function, decreasing *instantaneously* from U_0 to zero, and if the valve is initially set at an effectively negative angle of attack, the immediate effect is to induce a δ-function or *impulsive* destabilizing moment, and hence a dynamic response involving an instantaneously developed destabilizing *angular velocity*. This initial angular velocity can be computed without consideration of vortex shedding; indeed, it requires implementation of the condition that no change in the net circulation about the airfoil occurs during the impulse.

In the present article we replace the objective function (maximum steady reverse-flow moment) of I by that of maximizing this instantaneous angular velocity. Because of the simplifying assumption of no vortex shedding, this quantity can be expressed as a functional of the camber, for an airfoil of zero thickness, and hence is suitable for application of the calculus of variations (Craggs 1973).

Aside from replacement of one objective function by another, the present format follows I quite closely. That is, after formulating the problem mathematically, we first solve it analytically in the case of an airfoil alone in an unbounded fluid. The resulting optimal shape has zero camber at its leading and trailing edges.

We then treat the case where there is an additional boundary in the form of a plane wall parallel to the incident flow direction. This problem can only be solved numerically, and computed results are given for various clearance/chord ratios. The limiting cases of large and small clearances are discussed.

Optimum shapes can be derived for any choice of the pivot point. However, we present here only those shapes that are in equilibrium for steady forward flow. A remarkable feature of these (highly cambered) shapes is that their centre of pressure coincides with that of a flat plate. Hence they are neutrally stable when in their equilibrium position. The influence of this property on actual design remains to be investigated.

The optimization is carried out subject to the constraint that the mean-square slope of the leaflet surface be held fixed. This constraint limits the extent to which the leaflet obstructs the forward flow when the valve is fully open. The relationship between this constraint and the pressure drop across the valve is discussed in §6. Further work is needed to quantify this relationship, and also to investigate the (possibly beneficial) effect of non-uniform leaflet thickness.

2. The general unsteady-flow problem

Our concern is with a two-dimensional flow about a zero-thickness airfoil with equation $y = h+\bar{f}(x,t)$, $-l < x < l$. The fluid is inviscid and incompressible and the flow irrotational except for a possible trailing vortex sheet. Thus its velocity can be written

$$\mathbf{q} = \nabla(U(t)\,x+\phi(x,y,t)), \tag{2.1}$$

where $U(t)$ is the time-varying uniform stream at infinity. That is, at infinity the disturbance velocity $\nabla\phi$ tends to zero.

Elsewhere, ϕ satisfies Laplace's equation, subject to the boundary condition

$$\frac{\partial\phi}{\partial y} = \frac{\partial\bar{f}}{\partial t}+\left(U+\frac{\partial\phi}{\partial x}\right)\frac{\partial\bar{f}}{\partial x} \tag{2.2}$$

on the airfoil $y = h+\bar{f}(x,t)\pm 0$. This condition is linearized to

$$\frac{\partial\phi}{\partial y} = \frac{\partial\bar{f}}{\partial t}+U\frac{\partial\bar{f}}{\partial x}, \tag{2.3}$$

and applied on $y = h\pm 0$ for airfoils at small local angles of attack $-\bar{f}_x$.

The remaining boundary conditions are vanishing normal velocity on the plane wall, i.e.

$$\frac{\partial\phi}{\partial y} = 0 \quad \text{on} \quad y = 0, \tag{2.4}$$

and continuity of pressure across the trailing wake vortex sheet for $x > l$. Bernoulli's equation gives the pressure as

$$p = -\rho\left(\frac{\partial\phi}{\partial t}+\tfrac{1}{2}q^2-\tfrac{1}{2}U^2\right). \tag{2.5}$$

This pressure is normalized so that its value at infinity is $-\rho\dot{U}(t)\,x$. Upon linearization, (2.5) gives

$$p = -\rho\left(\frac{\partial\phi}{\partial t} + U\frac{\partial\phi}{\partial x}\right), \tag{2.6}$$

and the linearized wake condition is therefore that there be no jump in $\phi_t + U\phi_x$ across the limiting plane vortex sheet $y = h \pm 0$, $x > l$. In fact this condition also applies at the trailing edge $x = l$, where it defines the 'Kutta' condition.

In the special case in which the airfoil is a rigid body capable of rotating about a pivot at $x = x_0$, we have

$$\bar{f}(x,t) = f(x) + \alpha(t)\,(x - x_0), \tag{2.7}$$

where $\alpha(t)$ is the angle of attack, for some given $f(x)$ function. Note that without loss of generality we may take $\alpha(0) = 0$, absorbing any initial angle of attack into the definition of the function $f(x)$. Now the boundary condition (2.3) becomes

$$\frac{\partial\phi}{\partial y} = \dot{\alpha}(t)\,(x - x_0) + U[f'(x) + \alpha(t)]. \tag{2.8}$$

Once the above boundary-value problem is solved for ϕ, we may compute the pressure using (2.6), and hence the elementary vertical force dF on a section dx of the airfoil, namely

$$dF = -[p(x, h+0, t) - p(x, h-0, t)]\,dx, \tag{2.9}$$

from which follows the moment about the hinge point

$$M(t) = \int_{-l}^{l} (x - x_0)\,dF. \tag{2.10}$$

Finally, the equation of motion is

$$I_0\ddot{\alpha}(t) = M(t), \tag{2.11}$$

where I_0 is the moment of inertia of the mass of the airfoil about $x = x_0$. The complete coupled dynamic–aerodynamic system so formulated must be solved simultaneously, i.e. as we advance the computation in time we use (2.11) to compute the new geometric position of the airfoil, before solving a new aerodynamic problem, etc.

3. Impulsive motion

When $U(t)$ changes rapidly, time rates of change $\partial/\partial t$ dominate convective rates of change $U\partial/\partial x$ in the above equations. Thus the pressure can be approximated as

$$p = -\rho\frac{\partial\phi}{\partial t}, \tag{3.1}$$

and the boundary condition (2.8) by

$$\frac{\partial\phi}{\partial y} = \dot{\alpha}(t)\,(x - x_0) + Uf'(x). \tag{3.2}$$

Since the 'wake' condition is now simply continuity of $\partial\phi/\partial t$ and hence of ϕ across $y = h$, there can be no change in the circulation around the airfoil during the period in which the impulsive change occurs, and there is, as yet, no wake present.

Further, the potential ϕ can be decomposed into separate contributions from the two terms in (3.2), writing

$$\phi(x, y, t) = \dot{\alpha}(t)\,\phi_{\dot{\alpha}}(x, y) + U(t)\,\phi_U(x, y). \tag{3.3}$$

Note that the coefficient potentials $\phi_{\dot{\alpha}}$, ϕ_U can be assumed time-invariant, a reflection of the fact that no 'history' effects can be present in the absence of vortex shedding. The boundary conditions satisfied by $\phi_{\dot{\alpha}}$ and ϕ_U are respectively

$$\partial\phi_{\dot{\alpha}}/\partial y = x - x_0, \tag{3.4}$$

$$\partial\phi_U/\partial y = f'(x). \tag{3.5}$$

A corresponding decomposition of pressure, force and moment gives

$$M(t) = -\ddot{\alpha}(t)\, I_A - \dot{U}(t)\,\mu, \tag{3.6}$$

where

$$I_A = -\rho \int_{-l}^{l} (x - x_0)\,[\phi_{\dot{\alpha}}(x, h+0) - \phi_{\dot{\alpha}}(x, h-0)]\,dx, \tag{3.7}$$

$$\mu = -\rho \int_{-l}^{l} (x - x_0)\,[\phi_U(x, h+0) - \phi_U(x, h-0)]\,dx. \tag{3.8}$$

The quantity I_A has the interpretation of an added moment of inertia. This is seen by writing the equation of motion (2.11) as

$$(I_0 + I_A)\,\ddot{\alpha} = -\dot{U}(t)\,\mu, \tag{3.9}$$

the combined coefficient of the angular acceleration being the sum of the inertia of the airfoil itself and the added inertia of the fluid that must move with the airfoil. Although the linearized equations of motion can *always* be displayed in the form (3.9), it is only for the impulse case that the coefficients I_A and μ are constants, independent of the past history of the motion.

Since I_A and μ are pure constants in the present case, the 'solution' of (3.9) can be written down immediately as

$$\dot{\alpha}(t) = \dot{\alpha}(0_-) - \left(\frac{\mu}{I_0 + I_A}\right)[U(t) - U(0_-)]. \tag{3.10}$$

In particular, if $U(t)$ is of a step-function character, (3.10) implies that there is a corresponding discontinuity in the *angular velocity* $\dot{\alpha}$ of the airfoil. In such a case, (3.10) applies *exactly* at $t = 0_+$; i.e. it determines the instantaneous stepwise change in angular velocity, immediately after the free-stream velocity jumps. Alternatively, (3.10) can be interpreted as an approximation for the response to any change in $U(t)$ that is sufficiently rapid for vortex shedding to be neglected.

In the present case, we are interested in the dynamics of the airfoil subsequent to a sudden loss of forward speed, i.e. when $U(0_-) = U_0 > 0$, and $U(0_+) = 0$. Then, if the airfoil was initially at rest, i.e. $\dot{\alpha}(0_-) = 0$, (3.10) states that

$$\dot{\alpha}(0_+) = U_0 \frac{\mu}{I_0 + I_A}. \tag{3.11}$$

Thus, for $\mu > 0$, a positive (i.e. closing) angular velocity develops instantaneously at $t = 0_+$, whenever the flow is suddenly stopped. The design task is to choose the airfoil shape function $f(x)$ such that this instantaneously developed angular velocity is maximized.

In applications such as to heart valves, flow deceleration is rapid, but of course not exactly instantaneous. In such a case, our model allows a rapid, but not exactly

instantaneous, development of a valve-closing angular velocity, with angular acceleration proportional to the flow deceleration $-\dot{U}(t)$.

It is notable that the quantity I_A is independent of f, and furthermore can be shown to be positive. Hence our task can be interpreted as that of maximizing the quantity μ defined by (3.8), by variation in f. This maximization is carried out subject (as in I) to the constraint of keeping fixed the mean-square slope

$$E = \frac{1}{2l}\int_{-l}^{l} f'(x)^2\,dx. \tag{3.12}$$

We perform this optimization for each separate choice of the pivot point x_0, finally hoping to choose that member of the family of optimum airfoils such that the steady forward flow is in equilibrium.

The boundary-value problems for ϕ_U and $\phi_{\dot{a}}$ can be solved in terms of distributions of vortices over the chord $y = h$, $-l < x < l$, together with their images in the plane wall $y = 0$. Thus for example

$$\phi_U(x,y) = \frac{1}{2\pi}\int_{-l}^{l} \gamma(\xi)\left[\arctan\frac{y-h}{x-\xi} - \arctan\frac{y+h}{x-\xi}\right]d\xi, \tag{3.13}$$

with branch cuts of the arctangent function taken downstream of the vortex points at $x = \xi$, and principal values taken on the interval $(-\pi,\pi)$. Upon substitution into the boundary condition (3.5), we obtain an integral equation for the unknown vortex strength $\gamma(x)$, namely

$$\int_{-l}^{l} \gamma(\xi)\,K(x-\xi)\,d\xi = f'(x), \tag{3.14}$$

where

$$2\pi K(x) = \frac{1}{x} - \frac{1}{x^2+4h^2}. \tag{3.15}$$

An identical integral equation holds for the $\phi_{\dot{a}}$ problem, with $f'(x)$ replaced by $x - x_0$.

The integral equation (3.14) must be solved subject to the zero-circulation condition

$$\int_{-l}^{l} \gamma(x)\,dx = 0. \tag{3.16}$$

Except in the limit as $h \to \infty$, to be treated in § 4, there is no analytic solution of (3.14), and we shall have to solve numerically. Once $\gamma(x)$ is determined, the potential jump follows as

$$\phi_U(x,h+0) - \phi_U(x,h-0) = -\int_{-l}^{x} \gamma(\xi)\,d\xi, \tag{3.17}$$

and hence the moment coefficient (3.8) is

$$\mu = -\tfrac{1}{2}\rho\int_{-l}^{l} (x-x_0)^2\,\gamma(x)\,dx. \tag{3.18}$$

4. Analytic solution for unbounded fluid

If $h = \infty$, the integral equation (3.14) has, as its exact solution subject to (3.16), the expression

$$\gamma(x) = -\frac{2}{\pi}(l^2-x^2)^{-\frac{1}{2}}\int_{-l}^{l} \frac{(l^2-\xi^2)^{\frac{1}{2}} f'(\xi)\,d\xi}{x-\xi}, \tag{4.1}$$

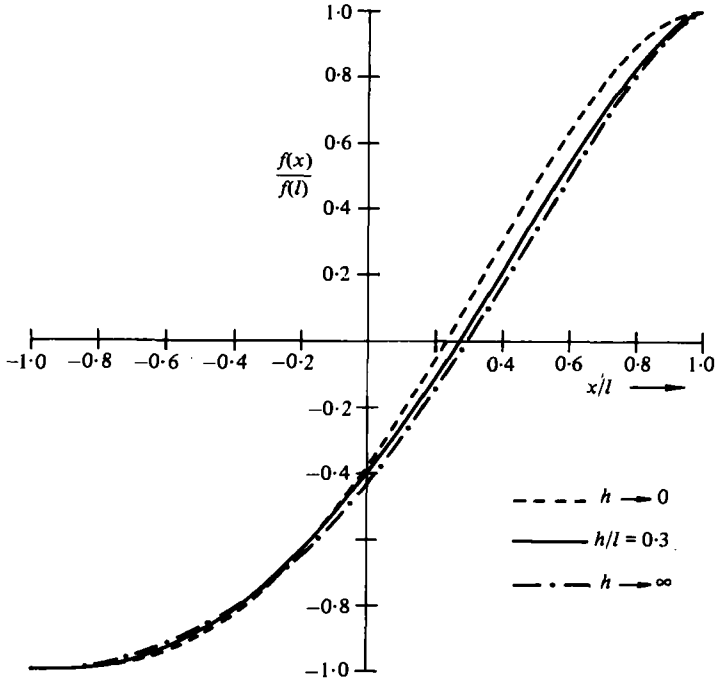

FIGURE 2. Optimal zero-thickness leaflets for $h/l = 0, 0{\cdot}3, \infty$.

from which (3.18) gives an explicit formula for the moment coefficient μ in terms of the airfoil slope function $f'(x)$, namely

$$\mu = \rho \int_{-l}^{l} (x - 2x_0)\,(l^2 - x^2)^{\frac{1}{2}} f'(x)\,dx. \tag{4.2}$$

For example, a flat plate at angle of attack α, with

$$f'(x) = -\alpha, \tag{4.3}$$

has

$$\mu = \rho\pi\alpha x_0 l^2. \tag{4.4}$$

Similarly, the choice $f'(x) = x - x_0$ in (4.2) gives the moment of inertia I_A, namely

$$I_A = \tfrac{1}{8}\rho\pi l^2[l^2 + 8x_0^2]. \tag{4.5}$$

Maximization of μ, subject to constancy of $\int f'^2\,dx$, implies immediately that f' is proportional to the kernel function in (4.2), i.e.

$$f'(x) = \lambda(x - 2x_0)\,(l^2 - x^2)^{\frac{1}{2}} \tag{4.6}$$

for some Lagrange multiplier λ, which simply provides the scale of the camber, and is clearly positive. The optimum airfoil thus has zero local angle of attack at both leading and trailing edges and (for $x_0 < 0$) maximum camber in its trailing half.

The resulting moment coefficient is

$$\mu = \tfrac{4}{15}\rho\lambda l^3(l^2 + 20x_0^2), \tag{4.7}$$

and the mean-square camber is

$$E = \lambda\mu/2\rho l. \tag{4.8}$$

The above optimization has been performed at fixed x_0. In fact our optimum solution is most useful if it is one that is in equilibrium for the steady forward flow. Now (as in I), in such a flow at speed U_0 the moment about $x = x_0$ is

$$M^+ = 2\rho U_0^2 \int_{-l}^{l} [l + x_0 - x] \left(\frac{l+x}{l-x}\right)^{\frac{1}{2}} f'(x)\, dx, \tag{4.9}$$

and if $f'(x)$ is given by (4.6) we have

$$M^+ = -4\rho U_0^2 \lambda l^2 x_0 (2x_0 + l). \tag{4.10}$$

Thus equilibrium can occur at $x_0 = 0$ or $x_0 = -\frac{1}{2}l$. The former position is clearly unstable, whereas the latter is at the critical position for static stability. That is, the present cambered airfoil with $x_0 = -\frac{1}{2}l$ has the remarkable property of having its centre of pressure at precisely the same (quarter-chord) position as does a flat plate at an angle of attack. If $x_0 = -\frac{1}{2}l$, (4.6) gives

$$f'(x) = \lambda(l+x)^{\frac{3}{2}}(l-x)^{\frac{1}{2}}. \tag{4.11}$$

Note that the leading edge not only has zero slope but also zero curvature. Its shape is shown in figure 2 as the curve for $h \to \infty$.

5. Numerical solutions for finite wall clearance

Although there is no explicit functional such as (4.2) to maximize when $h < \infty$, it is still possible to apply the methods of the calculus of variations (Craggs 1973). That is, if we wish to maximize μ given by (3.18), subject to constancy of E given by (3.12), and a zero value of the net circulation given by (3.16), variations $\delta f'$ in $f'(x)$ and $\delta\gamma$ in $\gamma(x)$ must satisfy

$$\int_{-l}^{l} [f'(x)\,\delta f'(x) + (\lambda_1(x-x_0)^2 + \lambda_2)\,\delta\gamma(x)]\, dx = 0, \tag{5.1}$$

for some Lagrange multipliers λ_1, λ_2. The variations $\delta f'$ and $\delta\gamma$ are connected by the integral equation (3.14), and hence we can eliminate $\delta f'(x)$, giving

$$\int_{-l}^{l} \left[\int_{-l}^{l} f'(\xi)\, K(\xi - x)\, d\xi + \lambda_1(x-x_0)^2 + \lambda_2 \right] \delta\gamma(x)\, dx = 0. \tag{5.2}$$

Since the variation $\delta\gamma(x)$ is arbitrary, and $K(-x) = -K(x)$, (5.2) implies

$$\int_{-l}^{l} f'(\xi)\, K(x-\xi)\, d\xi = \lambda_1(x-x_0)^2 + \lambda_2. \tag{5.3}$$

Equation (5.3) is now interpreted as an integral equation to determine the required slope function $f'(x)$. It is, of course, identical to the equation (3.14) that determines the vorticity, for a quadratically varying slope function. Any numerical procedure for solving the flow problem yields immediately a solution of the optimal design problem.

However, we must take into account the fact that singular integral equations such as (3.14) and (5.3) require one additional condition to render their solutions unique. In the case of (3.14), that condition is the zero-circulation condition (3.16). In the case

of (5.3) the unknown is the geometrical quantity $f'(x)$, not $\gamma(x)$, and such a condition is no longer appropriate.

It is of importance that we have two arbitrary constants λ_1, λ_2 on the right of (5.3). Thus a total of three subsidiary conditions are needed. One of these is simply the choice of scale of the design, i.e. a multiplying factor like λ in §4, that ultimately determines the mean-square slope E.

The remaining two subsidiary conditions are chosen as

$$f'(\pm l) = 0. \tag{5.4}$$

That is, we require the airfoil to have zero slope at both of its edges, in its design configuration. This is consistent with the results obtained in §4 for the unbounded-fluid case. It is notable that any solution of (5.3) that does *not* satisfy (5.4), necessarily has a singularity of inverse-square-root character at the ends. That is, if the end slope of the optimum airfoil is not zero, it is necessarily infinite. Such a singularity causes the integral (3.12) for E to fail to converge, and (cf. I) although this is not necessarily an indication of failure of the design, it may be considered undesirable in practice.

The procedure for solving the integral equation (5.3) is described in I, and can be repeated almost unchanged here. The program automatically ensures that $f'(l) = 0$, and we simply enforce $f'(-l) = 0$ as well, by appropriate choice of the constants λ_1, λ_2. This solution can be carried out for any choice of the hinge point x_0, and we observe that the camber function f depends linearly on x_0; in particular, a term $\lambda_1 x_0^2$ on the right of (5.3) can be absorbed into the arbitrary constant λ_2.

The moment M^+ about the hinge point $x = x_0$ during steady forward flow at speed U_0 can then be determined by solving yet again an integral equation of the form (3.14), with $f'(x)$ given by the now-determined optimal camber. However, this steady-flow solution (say $\gamma = \gamma^+(x)$) must *not* satisfy (3.16), but rather the Kutta condition

$$\gamma^+(l) = 0 \tag{5.5}$$

at the forward-flow trailing edge $x = l$.

Then the required moment is (cf. I)

$$M^+ = -\rho U_0 \int_{-l}^{l} (x - x_0)\gamma^+(x)\,dx. \tag{5.6}$$

Since f' (and hence γ^+) is a linear function of x_0, M^+ is quadratic in x_0, and can be written (as in (4.10)) as

$$M^+ = M_0 x_0(x_0 - x_1), \tag{5.7}$$

since it is clear by symmetry that $M^+ = 0$ if $x_0 = 0$. Computations at two separate values of x_0 enable estimation of the unknowns M_0 and x_1 in (5.7).

The method discretizes the interval $(-l, l)$ into N segments and inverts an $N \times N$ matrix. The error decays like N^{-2} as $N \to \infty$, and is below 0·5 % for all $N > 30$. The results show that, to at least this accuracy, the point $x = x_1$ coincides for all h with the point of neutral stability for steady forward flow. That is, $x = x_1$ is the centre of pressure of a flat plate at positive angle of attack in such a flow. Furthermore (cf. (4.10)), the solutions with $x_0 = x_1$ have $f''(-l) = 0$; i.e. the leading-edge curvature of the airfoil is zero.

This is a remarkable result. Except in the limiting cases $h \to \infty$ and $h \to 0$, we have not been able to prove it analytically, but the numerical evidence is strong. That is,

we are able to construct a family of cambered airfoils of zero thickness, which maximize the impulsively developed angular velocity of closing when the flow is reduced, but which are in *neutrally stable* equilibrium for steady forward flow.

The numerical results show only a very small variation in the optimal camber, as the clearance ratio h/l varies. Figure 2 gives $f(x)$ (scaled so $f(\pm l) = \pm 1$) for $h/l = 0{\cdot}3$ and for the limiting cases $h \to 0$ and $h \to \infty$. The curve for $h \to \infty$ corresponds to (4.11), and that for $h \to 0$ is the quartic polynomial with slope

$$f'(x) = \lambda(l+x)^2(l-x), \tag{5.8}$$

as can be verified by allowing $h \to 0$ in the integral equation (5.3). Shapes for all h/l interpolate smoothly between these limits (5.8), (4.11) as h varies from 0 to ∞, while the equilibrium pivot point varies between $-\frac{1}{3}l$ and $-\frac{1}{2}l$ (cf. figure 2 of I). This lack of sensitivity to clearance from the wall is quite encouraging, as it implies that an almost-universal camber function can be used for many possible design configurations. Note again that the actual vertical scale of figure 2 is arbitrary. The actual choice of the scale of $f(x)$ is necessarily a compromise between rate of closing and forward-flow obstruction; this is discussed further in §6.

Although the camber of the present theory is not unlike that developed in I on the basis of maximizing the steady reverse-flow moment, there are significant differences near the leading edge. The family in I had its maximum slope at that point, whereas in the present case not only the slope, but also its derivative, the curvature of the mean surface, should be zero at the leading edge. The analysis in I also included a non-zero airfoil thickness when $h < \infty$, whereas in the present computations we have taken the thickness as zero.

The fact that the forward-flow equilibrium pivot point is exactly neutrally stable is not necessarily a difficulty, although corrections allowing a reserve of stability may degrade the optimum. One obvious solution is to pivot slightly ahead of the equilibrium point $x_0 = x_1$. In that case (since M_0 in (5.7) is negative) there will be a small negative moment M^+ about the pivot point, so tending to cause the valve to open too far in the steady forward flow.

There are then two alternatives; either to resist this tendency, or not to. That is, the valve may be stopped from opening beyond the design position. In any case, this is the normal procedure in design of uncambered leaflets, for example as reviewed by Bonchek (1981) for prosthetic heart valves. In this case, the design can be the optimum for the given x_0, and will be slightly different from that shown for $x_0 = x_1$ in figure 2. Alternatively, we may allow the valve to open more, until it reaches equilibrium. Again, the optimum valve shape cannot be one of those in figure 2, since these are in equilibrium at $x_0 = x_1$. Further work is needed to clarify such 'slightly off-design' considerations.

6. Discussion

The leaflet shapes of figure 2 maximize the unsteady moment coefficient μ defined by (3.6), subject to fixed mean-square slope E as defined by (3.12), and a fixed hinge point x_0. The actual value of x_0 is chosen so that the steady forward flow is in equilibrium, and this value appears to coincide with that for which this equilibrium is exactly neutrally stable. For any fixed x_0, the moments of inertia (natural and added) are fixed, and hence maximum μ implies maximum initial rate of closing.

The choice of E as a constraint is dictated mainly by considerations of convenience, for application of the methods of the calculus of variations. The root-mean-square slope $E^{\frac{1}{2}}$ can be thought of as an averaged or effective angle of attack. Clearly we can increase the rate of closing as much as we like by increasing this effective angle of attack. The price to be paid for such an increase is an increase in the obstruction caused to the steady forward flow. Thus if, as is usually the case, we have to compromise in design by keeping this obstruction as small as possible, while maximizing the rate of closing, a constraint on E is quite appropriate.

In fact, this concept may be made a little more precise. An important design parameter for prosthetic heart valves is the 'pressure loss' due to their insertion in steady forward flow. That is, if we wish to maintain the same speed of flow in a tube containing a fully open valve as in one containing no valve at all, we must supply a small increase Δp in the pressure difference along the tube. It is conventional to use this quantity Δp as one of the figures of merit to compare different valves, i.e. a valve with a smaller Δp is 'better'.

It is hardly feasible to estimate Δp theoretically. In particular, $\Delta p = 0$ if the fluid is truly inviscid. One may expect that Δp is proportional to the *drag coefficient* C_{D} of the fully open leaflet. Thus, one empirical approach would be to use standard aerodynamic data on the drag of airfoils, e.g. from Abbott & Von Doenhoff (1959). In general, the drag $C_{\mathrm{D}} = C_{\mathrm{D}}(\alpha)$ on an airfoil of *fixed* camber can be written as a quadratic expression of the form

$$C_{\mathrm{D}}(\alpha) = C_{\mathrm{D}}(0) + \tfrac{1}{2}\alpha^2 C_{\mathrm{D}}''(0) \tag{6.1}$$

for small angle of attack α. The constant term $C_{\mathrm{D}}(0)$ is mainly skin friction; the term in α^2 can come from a variety of causes, such as shifts with α in the point of separation, blockage in the tube, induced drag, etc. More generally, if we consider a family of airfoils of various angles of attack and camber, it is not unreasonable to replace α^2 in (6.1) by the quantity E, which reduces to α^2 if the airfoil is uncambered.

Now if we vary the camber, the constant term $C_{\mathrm{D}}(0)$ is unchanged, so that drag variation occurs via variation in α^2, or equivalently in E. Thus we see that our constraint on E is quantitatively equivalent to a constraint on the pressure loss Δp, and when we compare the rate of closing of two valves with the same E we are in effect comparing them at fixed pressure loss. The leaflet shapes shown in figure 2 are guaranteed to be the best possible, for rate of closure, among families of fixed E, and therefore of fixed Δp.

For example we may wish to compare the present cambered leaflets with uncambered ones, i.e. with a simple flat plate at a suitable angle of attack α. If in fact we compare the ratio $\mu/E^{\frac{1}{2}}$, the effect is to eliminate the scales of the two leaflets, namely the angle of attack α of the flat plate, and the Lagrange multiplier for the optimal cambered leaflet (e.g. λ in (4.11)).

Even more appropriate is a comparison using the non-dimensional ratio

$$\Omega = \frac{l\mu}{E^{\frac{1}{2}} I_{\mathrm{A}}}, \tag{6.2}$$

where I_{A} is the added mass defined by (3.7). The quantity I_{A} can easily be computed using the present computer program, for any clearance ratio h/l. A useful property of the quantity Ω is that in some reasonable circumstances it approximates the actual

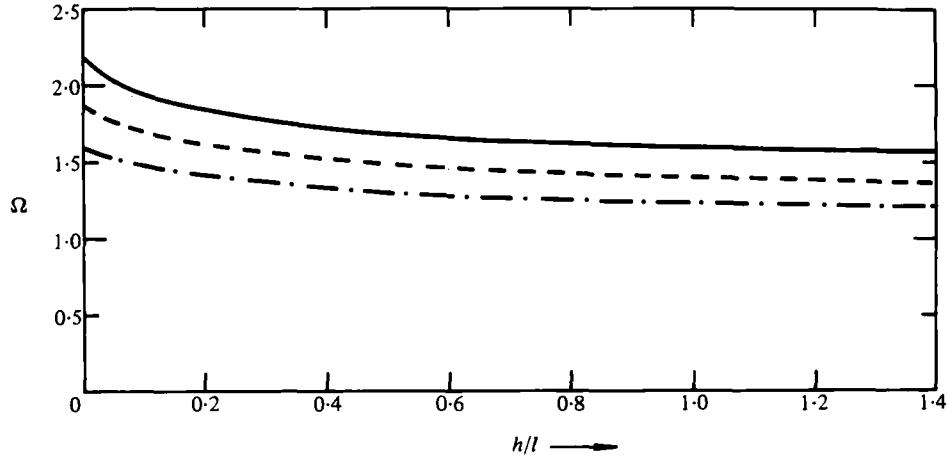

FIGURE 3. Scaled unsteady moment, or initial angular velocity of closing. The solid line is for the optimal cambered leaflets of figure 2, and the dashed line for a flat plate fixed at such an angle of attack as to yield the same mean square slope as the cambered leaflet. Also shown (chain-dotted) is the result for a flat plate whose angle of attack is the same as that of the chord line of the cambered leaflet.

rate of closing. Specifically, if we neglect the natural inertia I_0 relative to I_A in (3.11), the initial angular velocity of closing is

$$\dot{\alpha}(0) = \frac{U_0 E^{\frac{1}{2}}}{l}\Omega. \tag{6.3}$$

Note that for fixed Ω, $\dot{\alpha}$ is proportional to the forward flow speed U_0 and to the effective angle of attack $E^{\frac{1}{2}}$, and inversely proportional to the overall scale l of the valve. Neglect of I_0 compared with I_A is a good approximation for light leaflets, e.g. those lighter than a circumscribing circular cylinder of fluid.

Figure 3 shows Ω as a function of clearance ratio h/l, for the optimal leaflet and for a flat plate (dashed). The improvement due to camber is almost independent of clearance, being about 14 % for all h/l values. The pivot point is always chosen as that for forward flow equilibrium.

It should be noted that the comparison in figure 3 is necessarily favourable to the optimal leaflet, since that is guaranteed by the calculus-of-variations approach to have a better $\mu E^{-\frac{1}{2}}$ value than any other shape. However, it is in fact a somewhat severe test of the optimum, since the flat plate with the same E value has an angle of attack much greater than that of the optimal leaflet. For example, a more-naive but still perhaps relevant comparison would be with the flat plate that has the same angle of attack as the *chord line* of the optimal leaflet, i.e. lies in the line drawn between its leading and trailing edges. This flat plate has only about half of the angle of attack of the one with the same E-value, and hence the improvement due to camber is doubled to 28 %, again almost uniformly with respect to h/l. The chain-dotted curve of figure 3 gives the Ω value for this case.

So long as the camber is of the right general character, performance improvements over a flat plate can be almost as good as that of the optimum. For example, the steady-reversed-flow optimal shapes of I lead to μ-values that are little reduced compared with the present unsteady optimal shapes, for the same chord-line angle of attack. Unfor-

tunately, it is impossible to compare these two optima at fixed E, since the shapes of I have $E = \infty$.

Figure 2 enables some discussion of the role of the clearance ratio h/l on design. It would appear that Ω increases as h/l decreases, and hence a small clearance ratio is desirable. Within reason this is probably true. However, the idea that E measures changes in drag coefficient and hence pressure drop Δp becomes less tenable as $h \to 0$, so this conclusion should be interpreted with caution. In any case, most designs will have the h/l ratio determined by other considerations.

For example, a recent prosthetic heart valve design is that of St Jude Medical Inc. (Bonchek 1981). This involves two symmetrically placed flat leaflets at $\pm 5°$ to the flow direction. The plane $y = 0$ is thus not so much an actual boundary of the flow as a plane of symmetry. The clearance ratio is about $h/l = 0{\cdot}3$, and the hinge point at about quarter-chord, $x_0 = -\frac{1}{2}l$. The result of figure 3 shows that there is a potential gain of 14 % in the rate of closing, without increase in pressure loss, if the flat plate is replaced by a suitably cambered shape.

All results in the present paper are for leaflets of zero thickness. It is possible, as in I, to incorporate a designed optimal thickness distribution, to improve the performance even more. This is significant only for relatively small values of the clearance, say $h/l < 0{\cdot}5$. For example, at $h/l = 0{\cdot}3$ preliminary computations suggest that a further 16 % improvement in the Ω-value could be achieved by careful shaping of the leaflet thickness. This question is left for further investigation.

All computations were carried out on a TRS-80 microcomputer, with some selective checking on a CDC Cyber 173. The authors thank Dr M. Haselgrove for the latter, and for some critical discussions. Support by the Australian–American Educational Foundation, by the Life Insurance Medical Research Fund of Australia and New Zealand, by the Clive and Vera Ramaciotti Foundation, and by the Australian Research Grants Committee, is gratefully acknowledged.

REFERENCES

Abbott, I. H. & Von Doenhoff, A. E. 1959 *Theory of Wing Sections*. Dover.

Bonchek, L. I. 1981 Current status of cardiac valve replacement: Selection of a prosthesis and indications for operation. *Am. Heart J.* **101**, 96–106.

Craggs, J. W. 1973 *Calculus of Variations*. George Allen & Unwin.

Tuck, E. O. 1982 Two-dimensional leaflet valves with maximum reverse-flow moment. *J. Engng Math.* **16**, 47–57.

Yeung, R. W. 1978 On the interactions of slender ships in shallow water. *J. Fluid Mech.* **85**, 143–159.